Supporting Information

pH/Thermosensitive Dual-Responsive Hydrogel Based Sequential Delivery for Site-Specific Acute Limb Ischemia Treatment

Teng Zhang,[#ab] Huan Ouyang,[#e] Shichen Liu, [ab] Lei Xiong, [b] Zhiwei Zhong, [a] Qingqing Wang, [b] Zhuang Qiu, [bd] Yajia Ding, [b] Weimin Zhou, *[a] and Xiaolei Wang,*[bc]

a. Department of Vascular Surgery, the Second Affiliated Hospital of Nanchang University, Nanchang University, Nanchang, Jiangxi, 330006 (P.R. China)
b. The National Engineering Research Center for Bioengineering Drugs and the Technologies, Institute of Translational Medicine, Nanchang University, Nanchang, Jiangxi, 330088 (P.R. China)
c. College of Chemistry, Nanchang University, Nanchang, Jiangxi, 330088 (P.R. China)
d. School of Public Health & Jiangxi Provincial Key Laboratory of Preventive Medicine, Nanchang, Jiangxi, 330088 (P.R. China)
e. Department of Vascular and Thyroid Surgery, Department of General Surgery, the First Affiliated Hospital of Anhui Medical University, Anhui Medical University, Hefei, Anhui, 230022 (P.R. China)
[*] Corresponding author
E-mail addresses: zwmsubmit@126.com (Weimin Zhou), wangxiaolei@ncu.edu.cn (Xiaolei Wang)

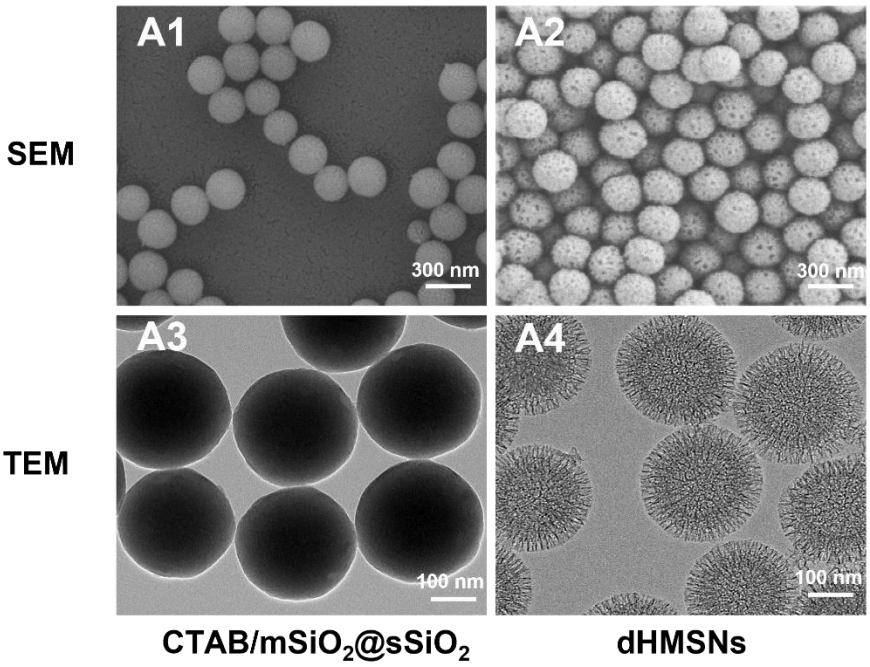

Figure S1. SEM images of (A1) CTAB/$mSiO_2$@$sSiO_2$ and (A2) dHMSNs. TEM images of (A3) CTAB/$mSiO_2$@$sSiO_2$ and (A4) dHMSNs.

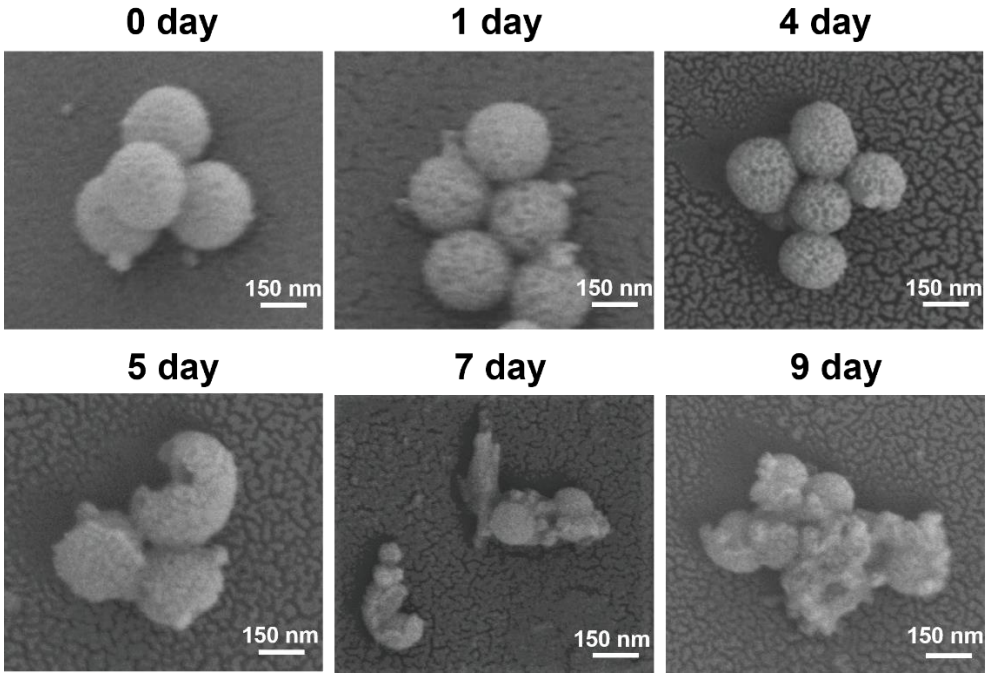

Figure S2. SEM images of dHMSNs at different degradation intervals in pH 7.4 PBS at 37 ℃.

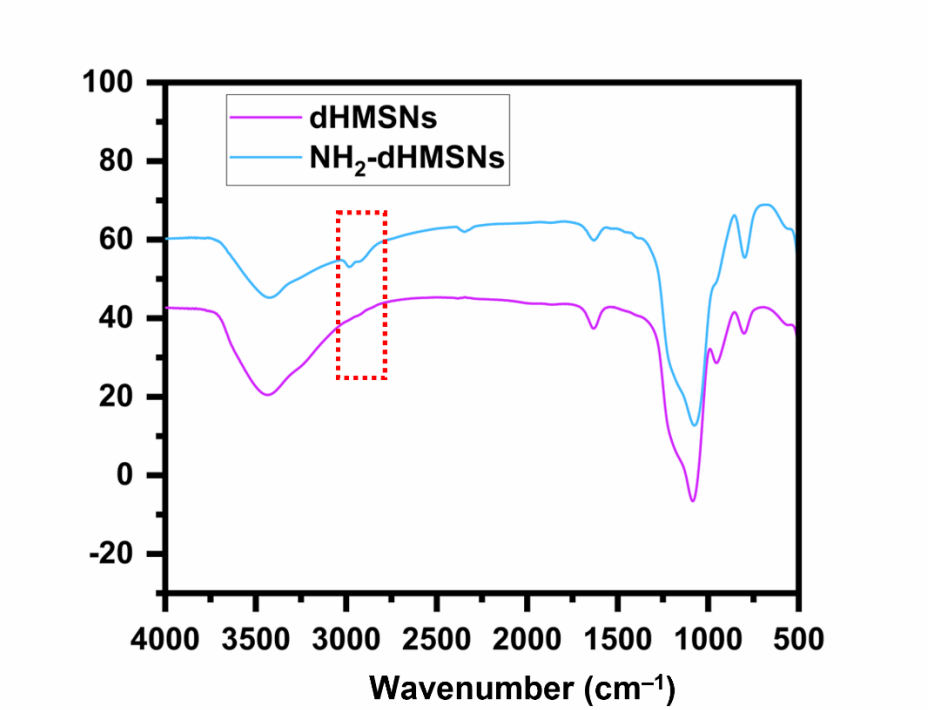

Figure S3. FTIR spectra of dHMSNs and NH_2-dHMSNs.

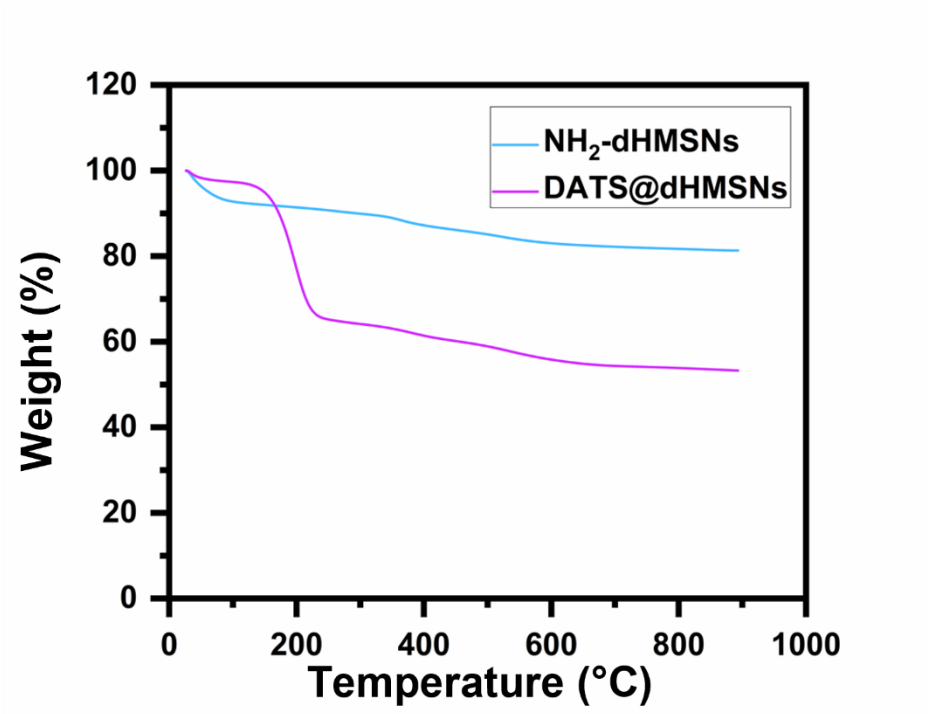

Figure S4. TG curves of NH_2-dHMSNs and DATS@dHMSNs.

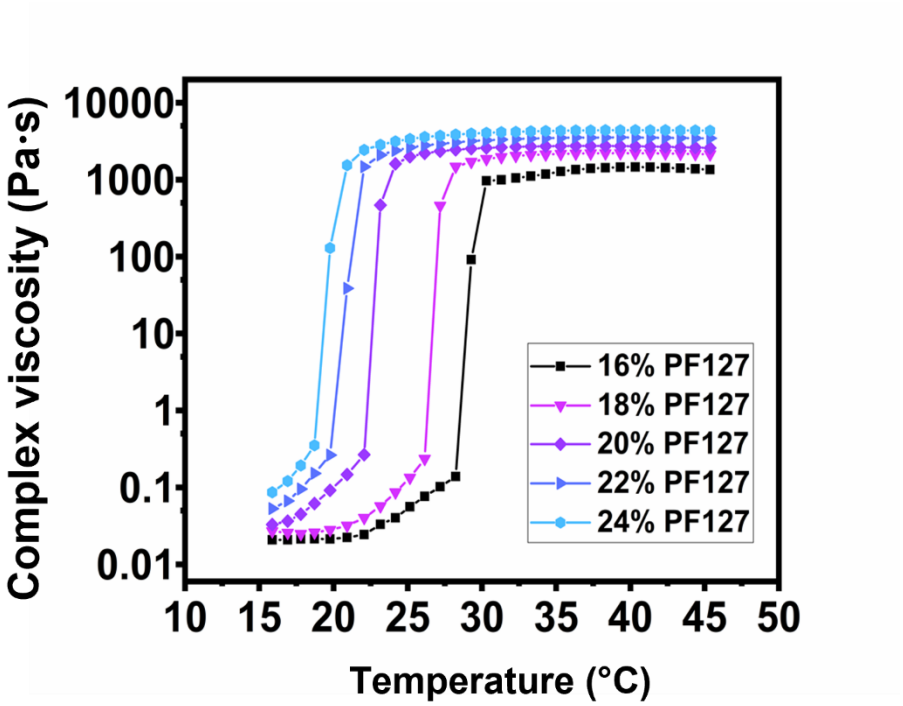

Figure S5. The complex viscosity (η) of PF127 at different concentrations (16%, 18%, 20%, 22% and 24%, respectively) altered with increasing temperature.

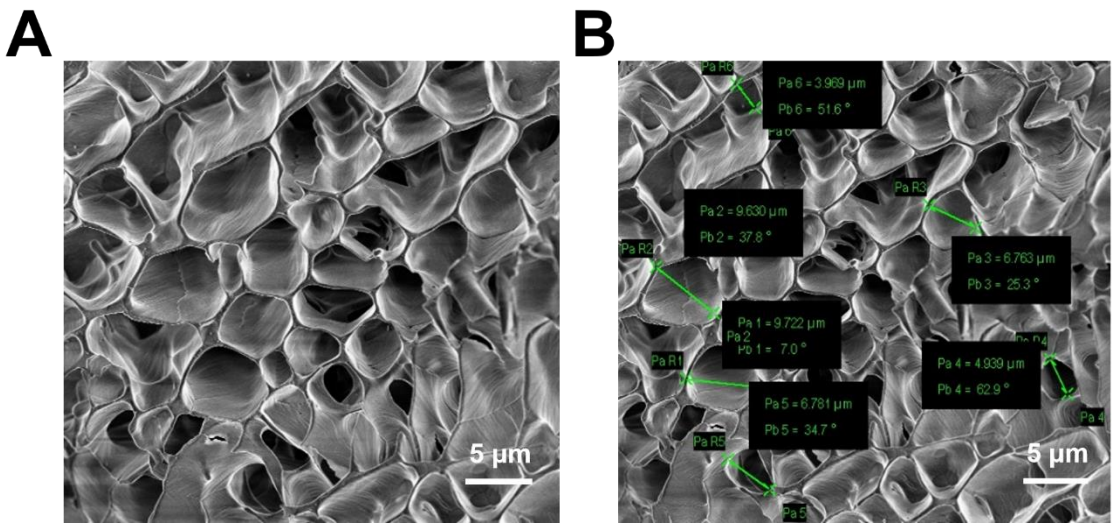

Figure S6. SEM images of PF127.

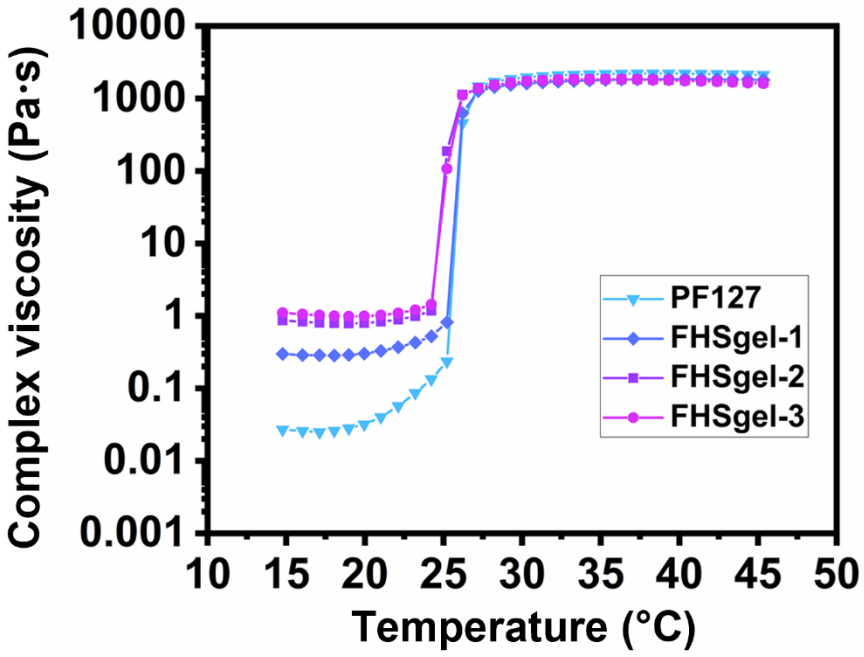

Figure S7. The complex viscosity (η) of 18% PF127 and FHSgel-1 (18% PF127: 0.5% HMPC: 0.5% SA), FHSgel-2 (18% PF127: 1% HMPC: 0.5% SA), FHSgel-3 (18% PF127: 0.5% HMPC: 1% SA).

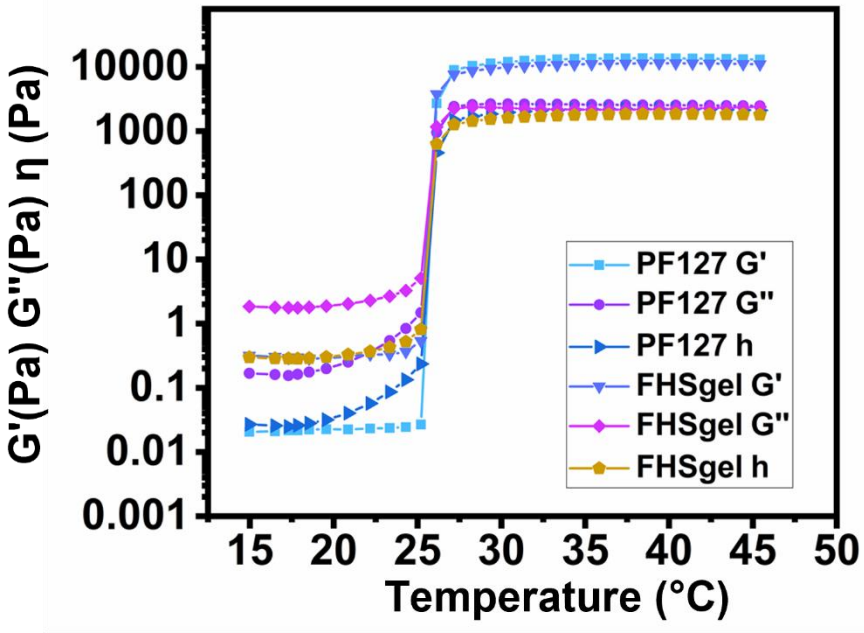

Figure S8. The total viscoelasticity including the storage modulus (G′), the loss modulus (G″) and the viscosity (η) of 18% PF127 and FHSgel (18% PF127: 0.5% HMPC: 0.5% SA).

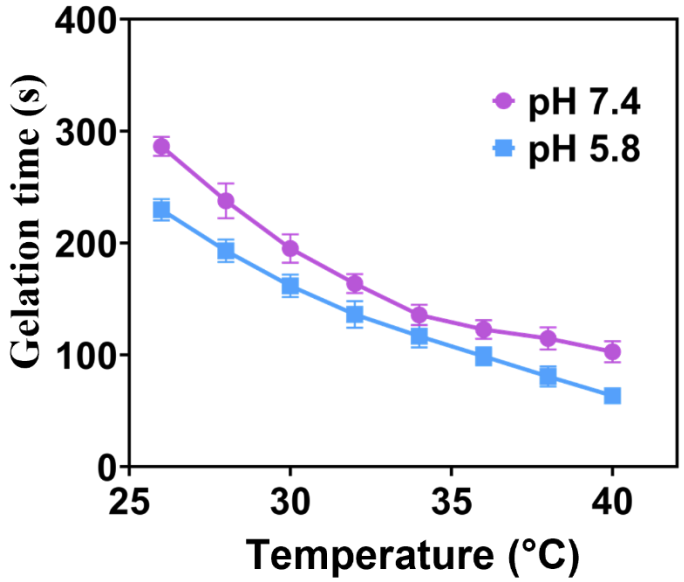

Figure S9. The gelation time changed with the increase of temperature in pH 7.4 and 5.8 PBS, respectively. Data are means ± s.d. (n = 3).

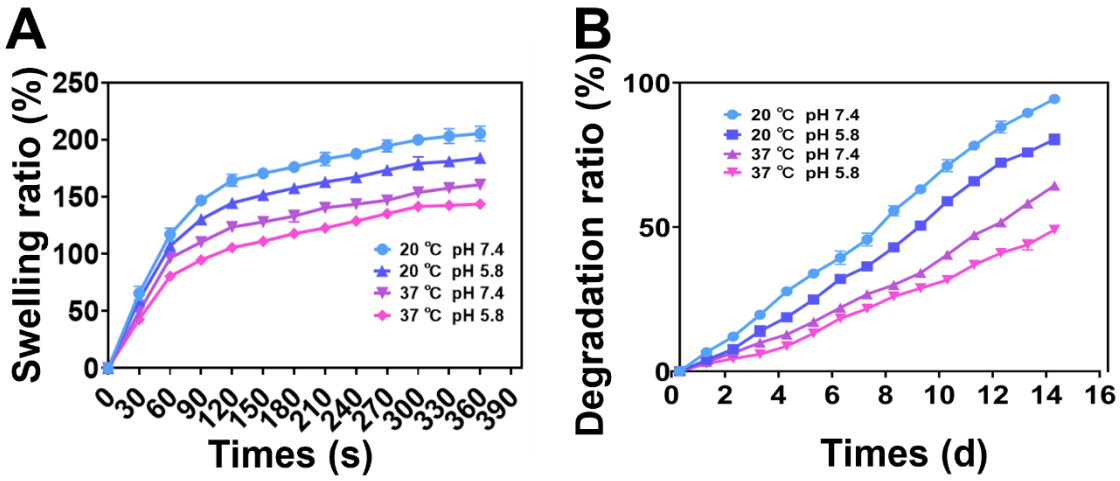

Figure S10. (A) swelling rate of FHSgel with different pH and temperatures; (B) degradation rate of FHSgel with different pH and temperatures. Data are means ± s.d. (n = 3).

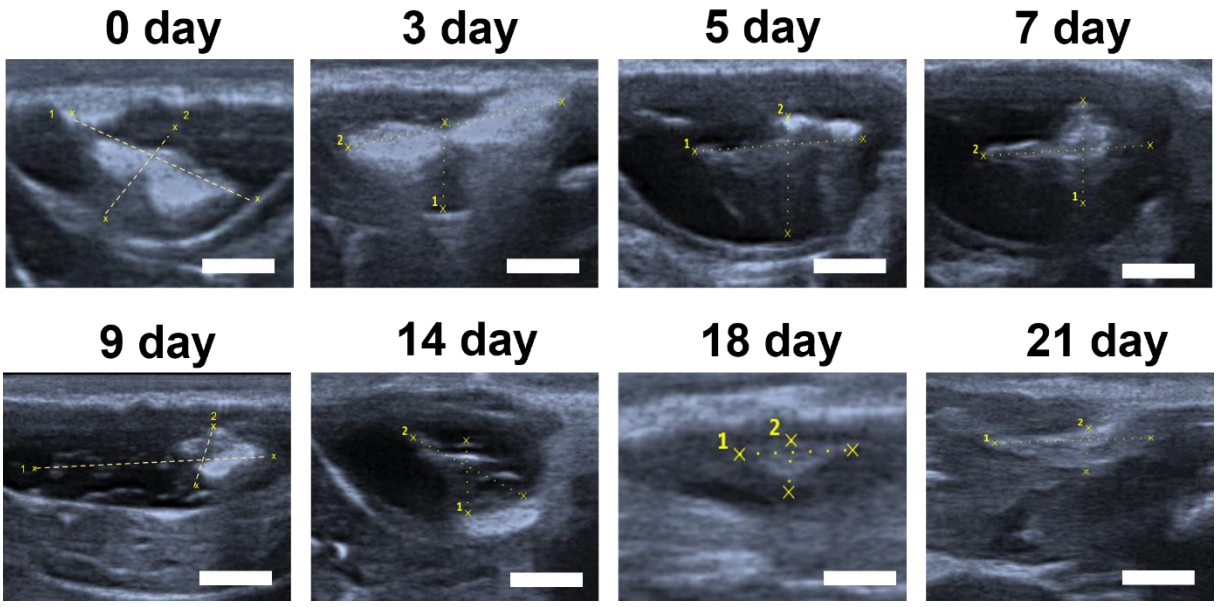

Figure S11. Ultrasound images of FHSgel degradation in rats (Scale bar = 2 mm).

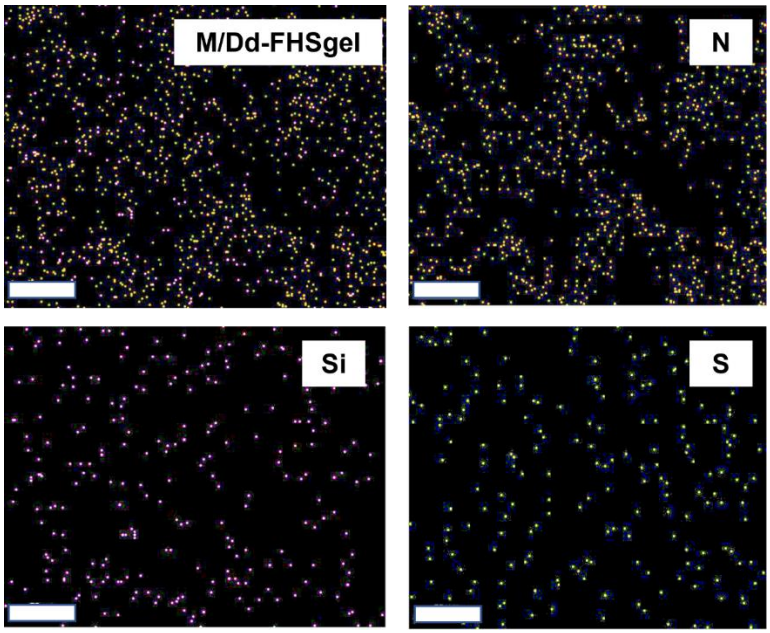

Figure S12. EDS images of M/Dd-FHSgel (Scale bar = 20 μm).

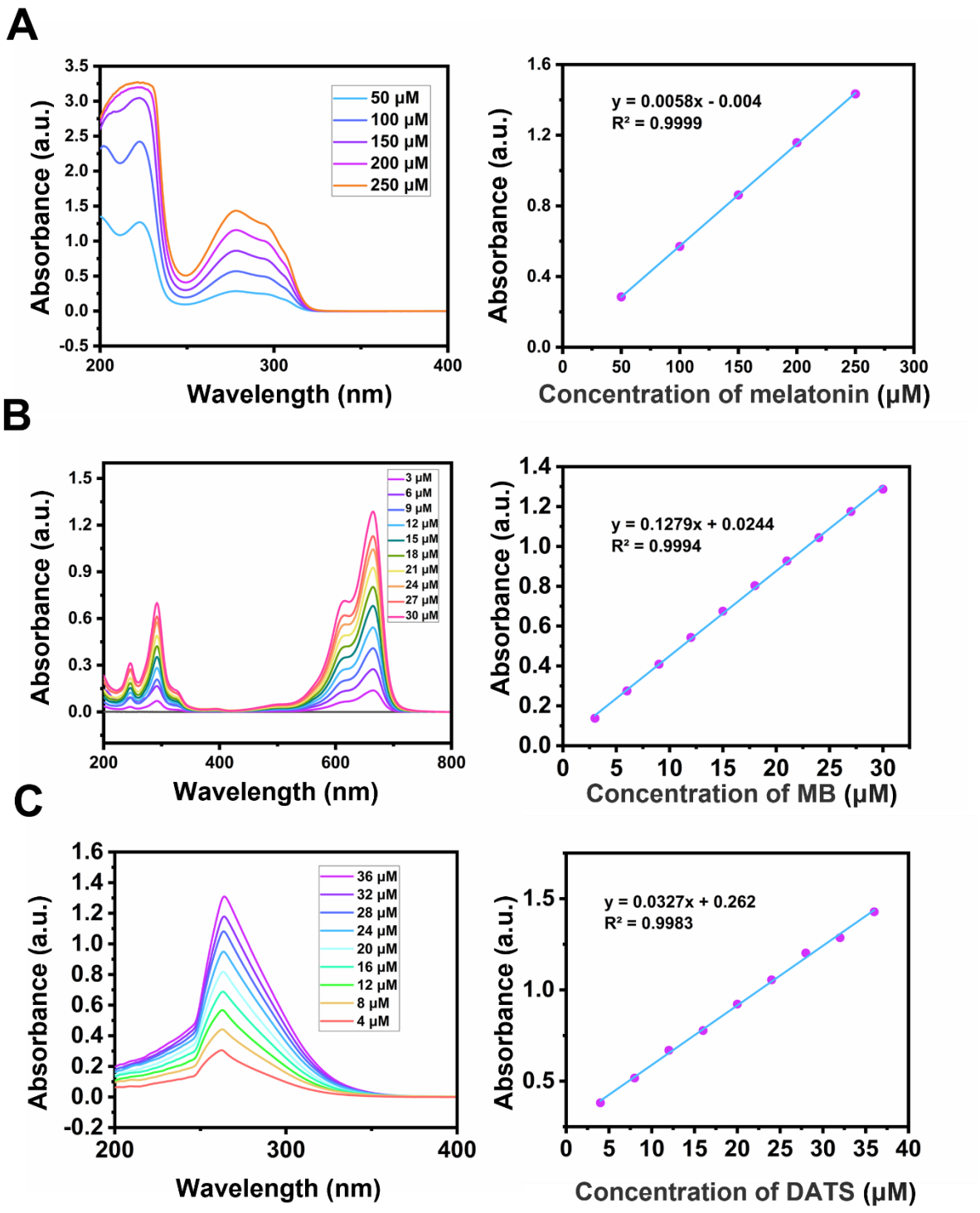

Figure S13. UV–vis absorption peaks and standard curves of (A) melation, (B) MB and (C) DATS.

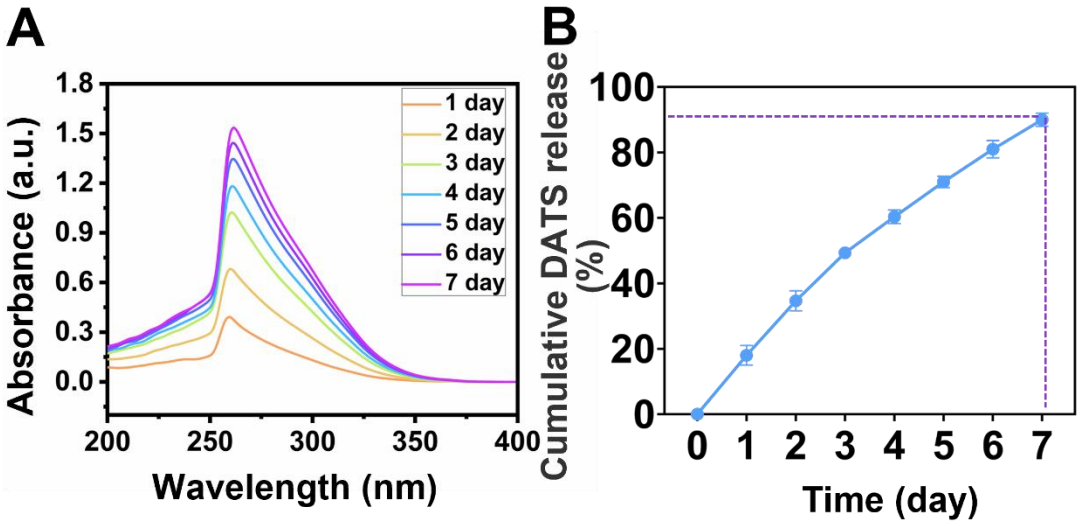

Figure S14. UV–vis absorption spectra of (A) DATS and (B) cumulative DATS release profile from DATS@dHMSNs in the absence of GSH in pH 7.4 PBS at different time. Data are means ± s.d. (n = 3).

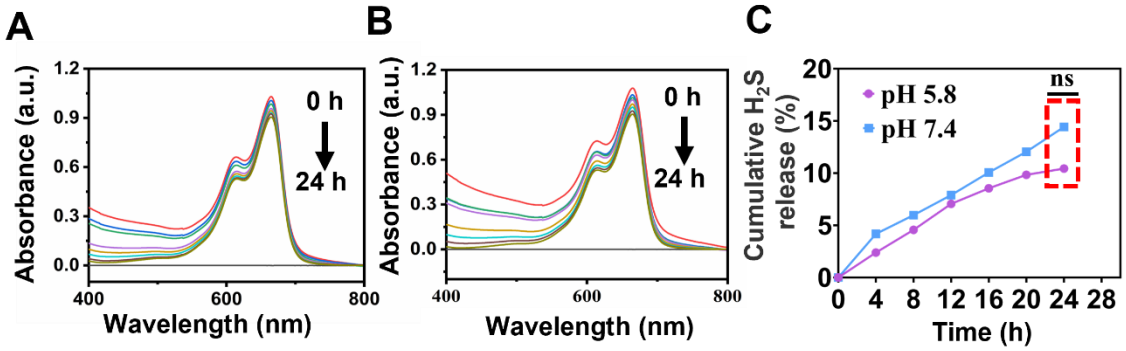

Figure S15. UV–vis absorption spectra of MB treated with DATS@dHMSNs and 2 mM GSH in (A) pH 5.8 and (B) 7.4 PBS at 37 ℃ and (C) cumulative H_2S release profiles at different time. *ns* represents no statistical difference.

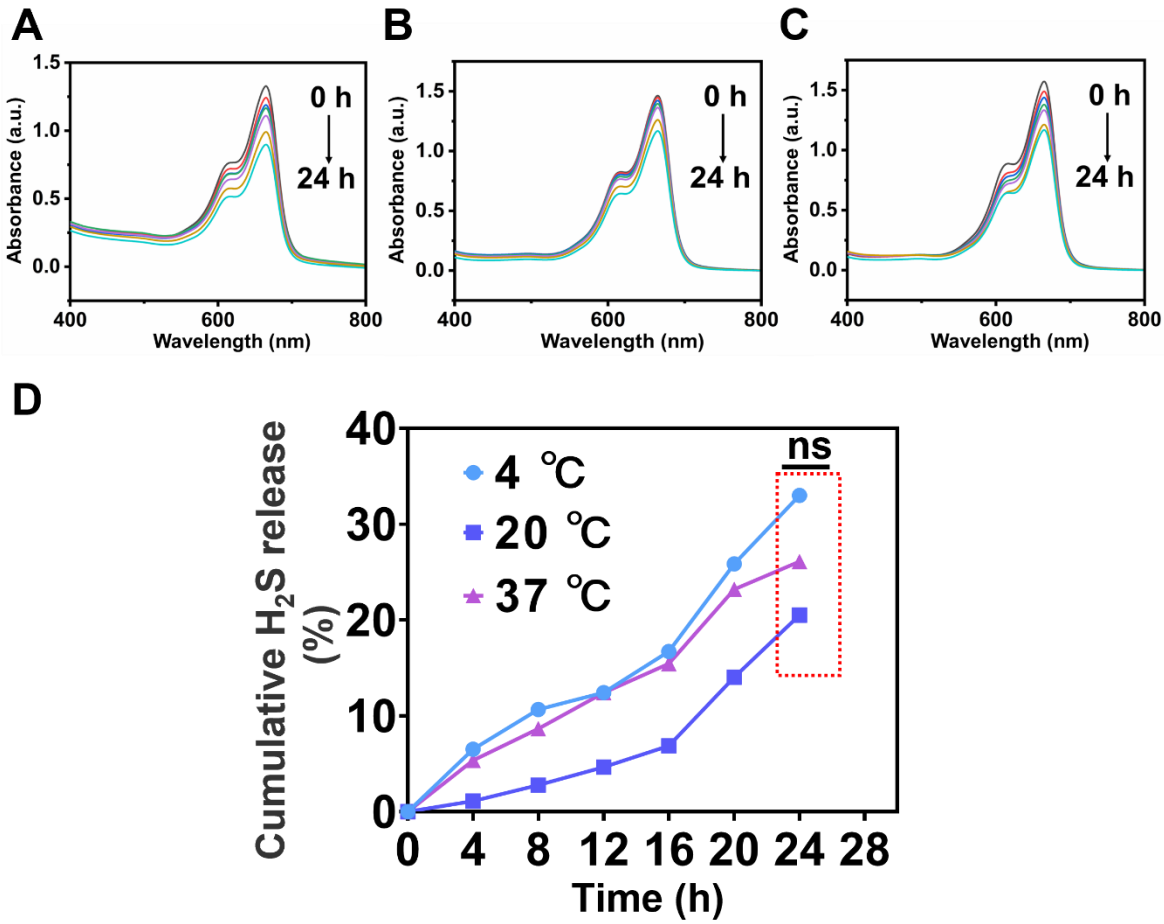

Figure S16. UV–vis absorption spectra of MB treated with DATS@dHMSNs and 2 mM GSH at (A) 4 ℃, (B) 20 ℃ and (C) 37 ℃ in pH 7.4 PBS, and (D) cumulative H_2S release profiles at different time. *ns* represents no statistical difference.

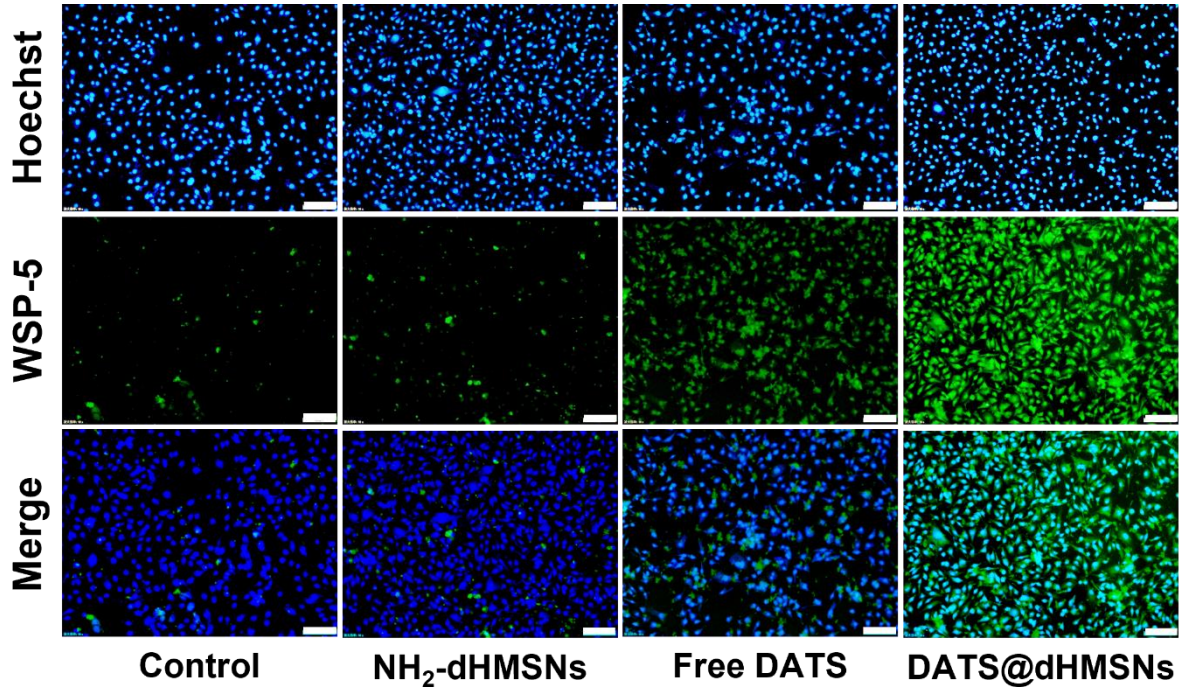

Figure S17. Fluorescence images of intracellular H_2S content in L929 detected by H_2S fluorescent probe (WSP-5, green channel) after 12 h coculture (Scale bar = 200 μm).

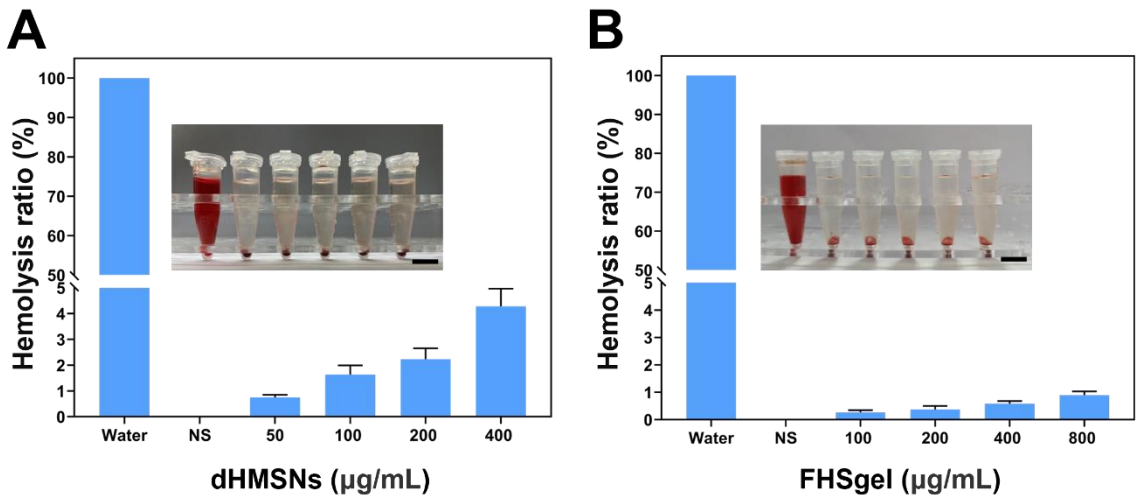

Figure S18. Hemolysis of red blood cells (RBCs) cocultured with different concentrations of (A) dHMSNs and (B) FHSgel (Scale bar = 1 cm). Data are means ± s.d. (n = 3).

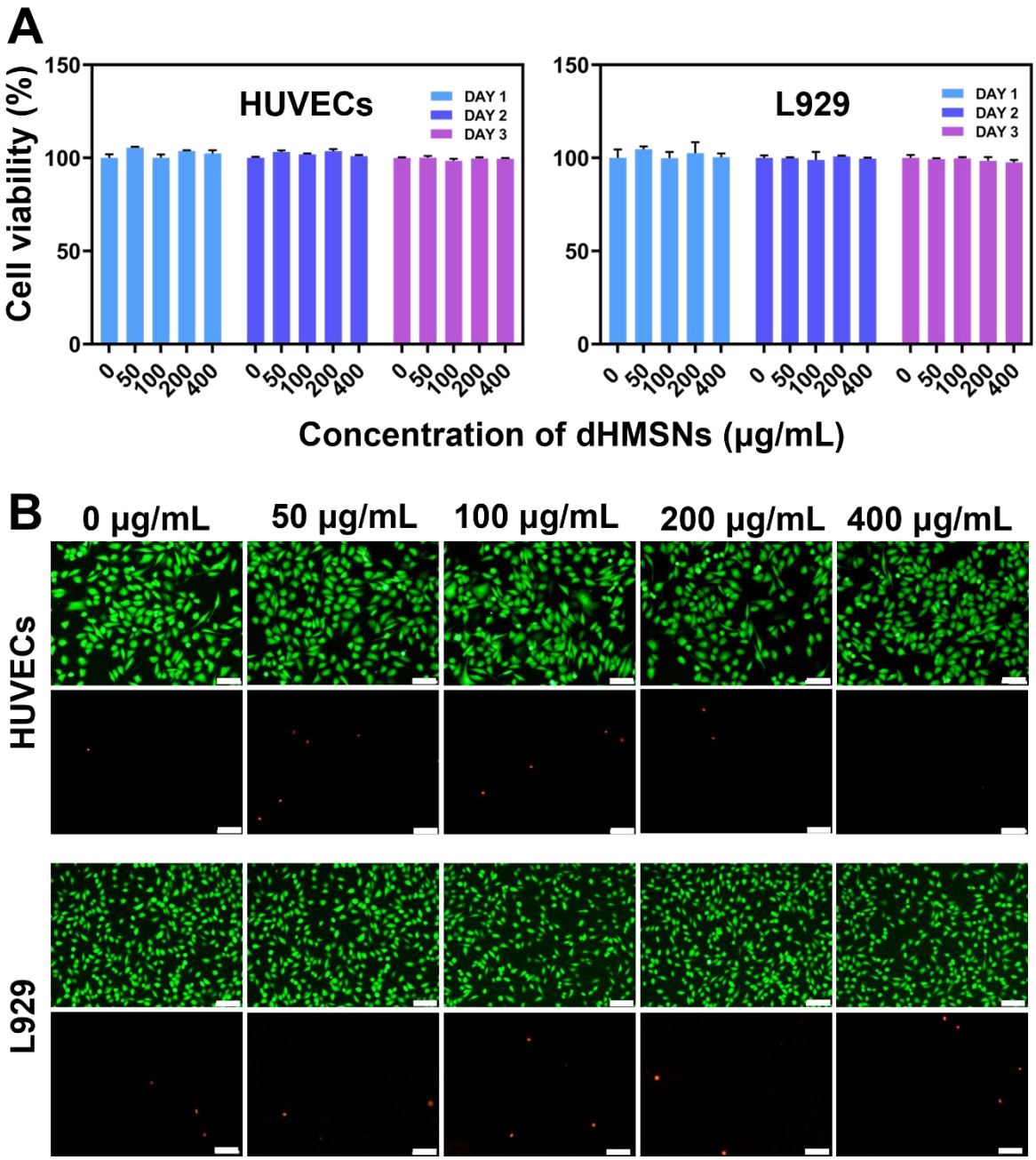

Figure S19. (A) Cytotoxicity of HUVECs and L929 cocultured with different concentrations of dHMSNs for 24 h, 48 h and 72 h. (B) Live/dead staining images of HUVECs and L929 after coculture with different concentrations dHMSNs for 72 h. Live/dead cells were stained with green and red fluorescent respectively (Scale bar = 100 μm). Data are means ± s.d. (n = 3).

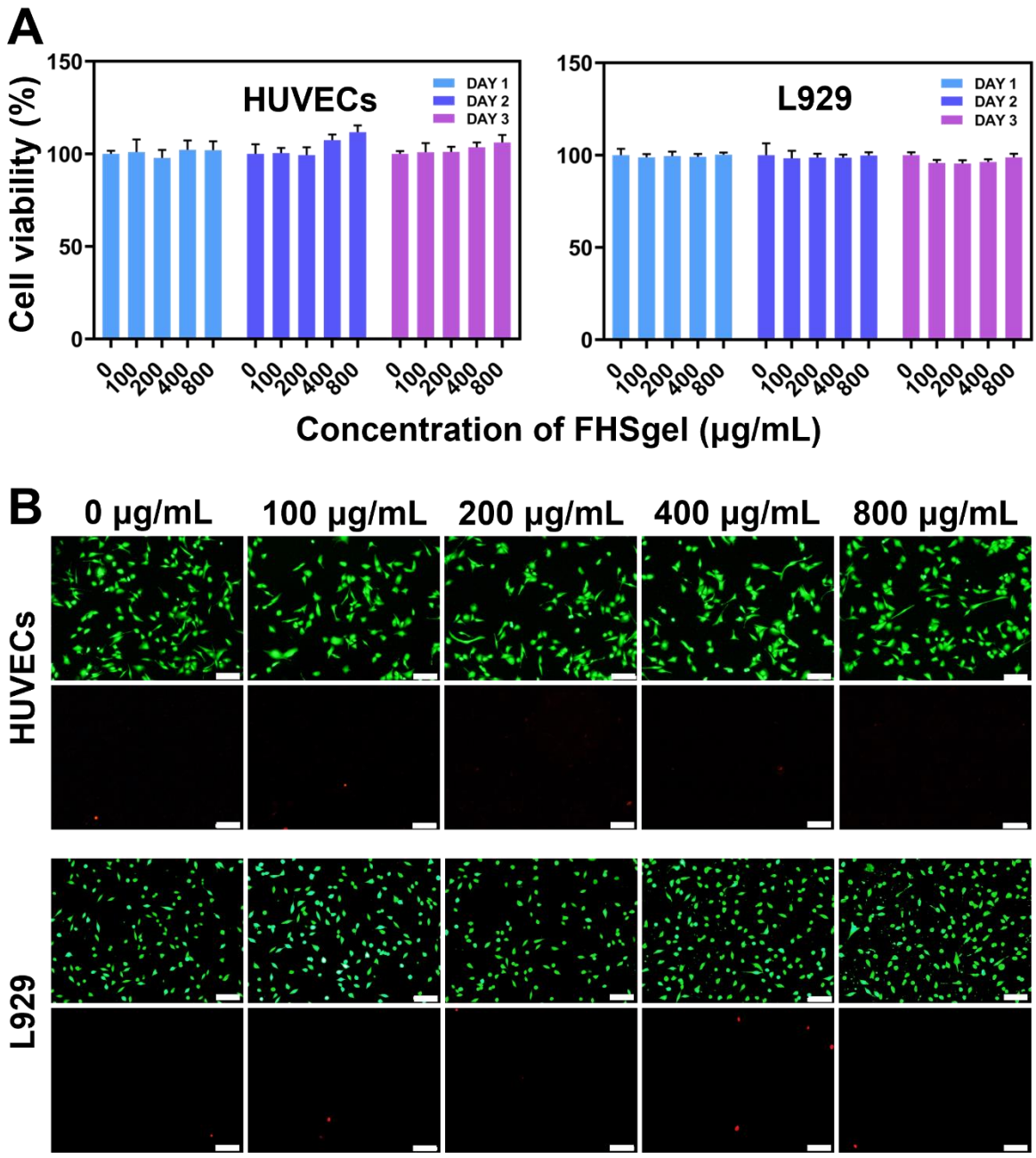

Figure S20. (A) Cytotoxicity of HUVECs and L929 cocultured with different concentrations of FHSgel for 24 h, 48 h and 72 h. (B) Live/dead staining images of HUVECs and L929 after coculture with different concentrations FHSgel for 72 h. Live/dead cells were stained with green and red fluorescent, respectively (Scale bar = 100 μm). Data are means ± s.d. (n = 3).

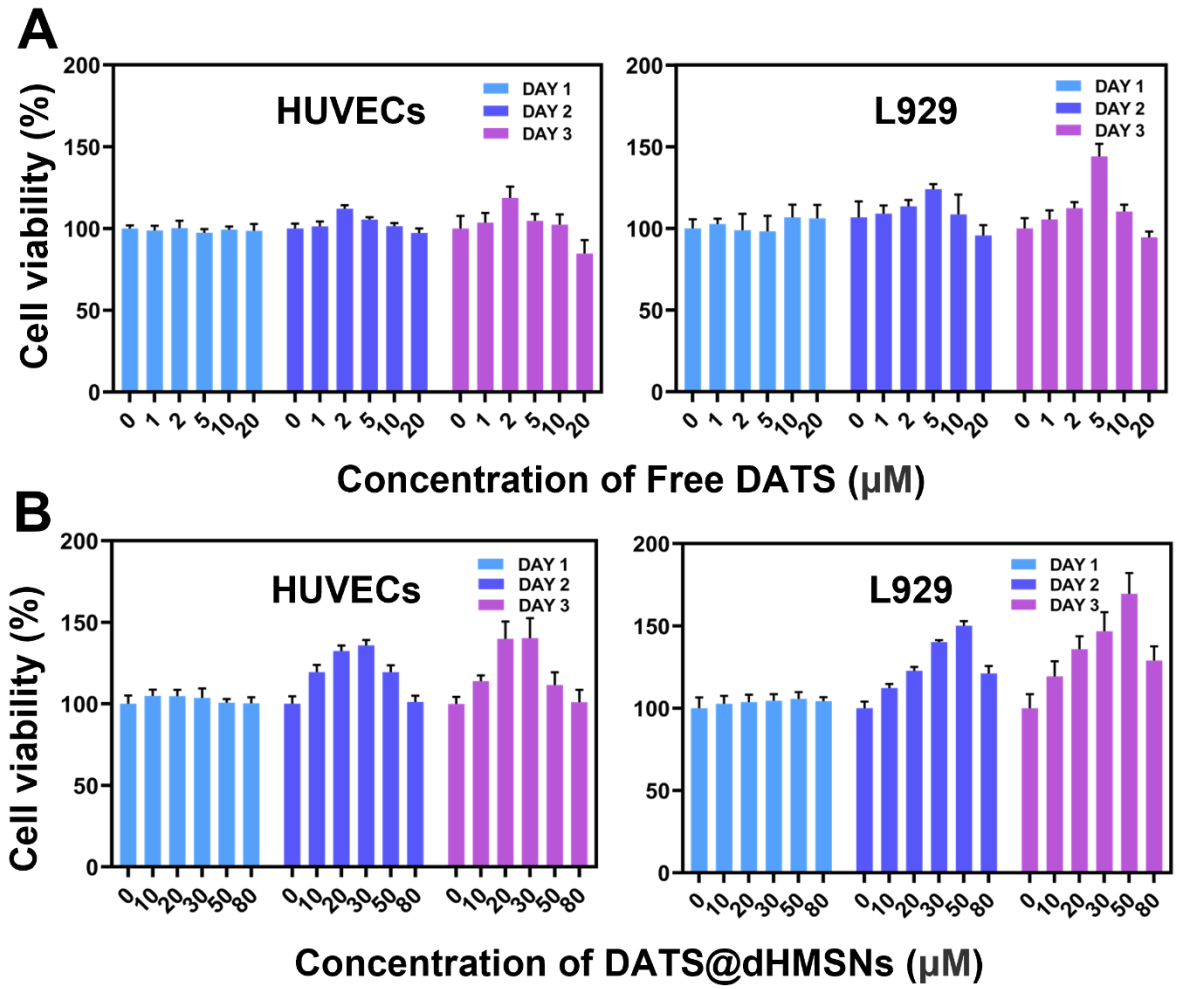

Figure S21. Cytotoxicity of HUVECs and L929 cocultured with different concentrations of DATS and DATS@dHMSNs for 24 h, 48 h and 72 h, respectively. Data are means ± s.d. (n = 3).

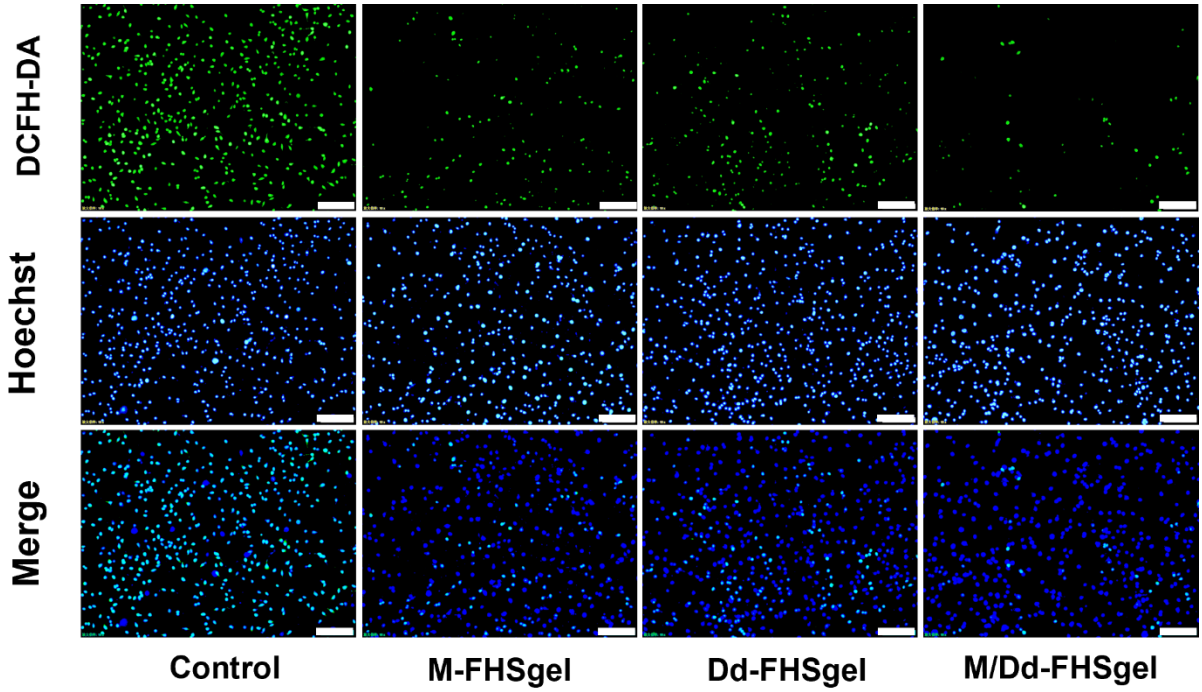

Figure S22. The intracellular ROS content of L929 with Control, M-FHSgel, Dd-FHSgel and M/Dd-FHSgel (Scale bar = 100 μm).

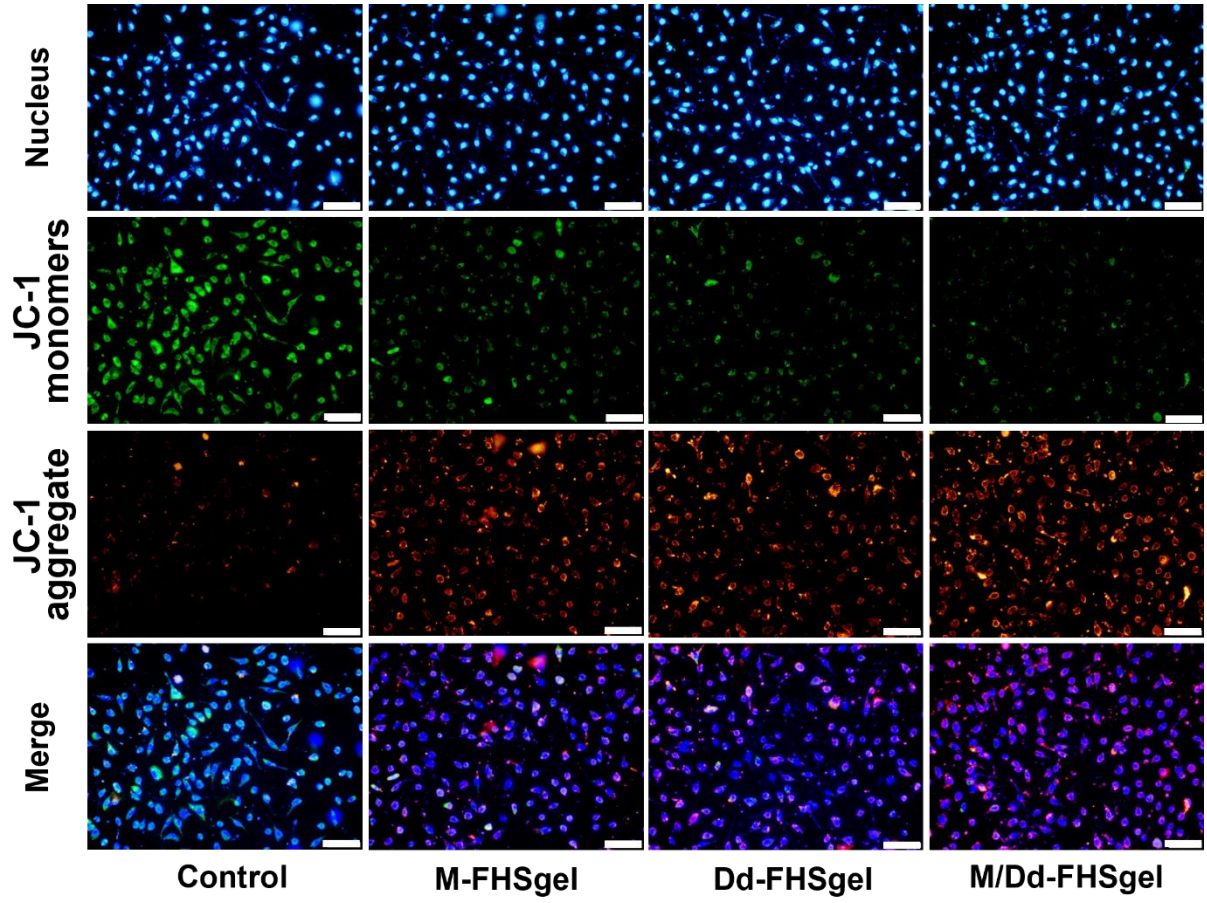

Figure S23. JC-1 staining of L929 with Control, M-FHSgel, Dd-FHSgel and M/Dd-FHSgel (Scale bar = 50 μm).

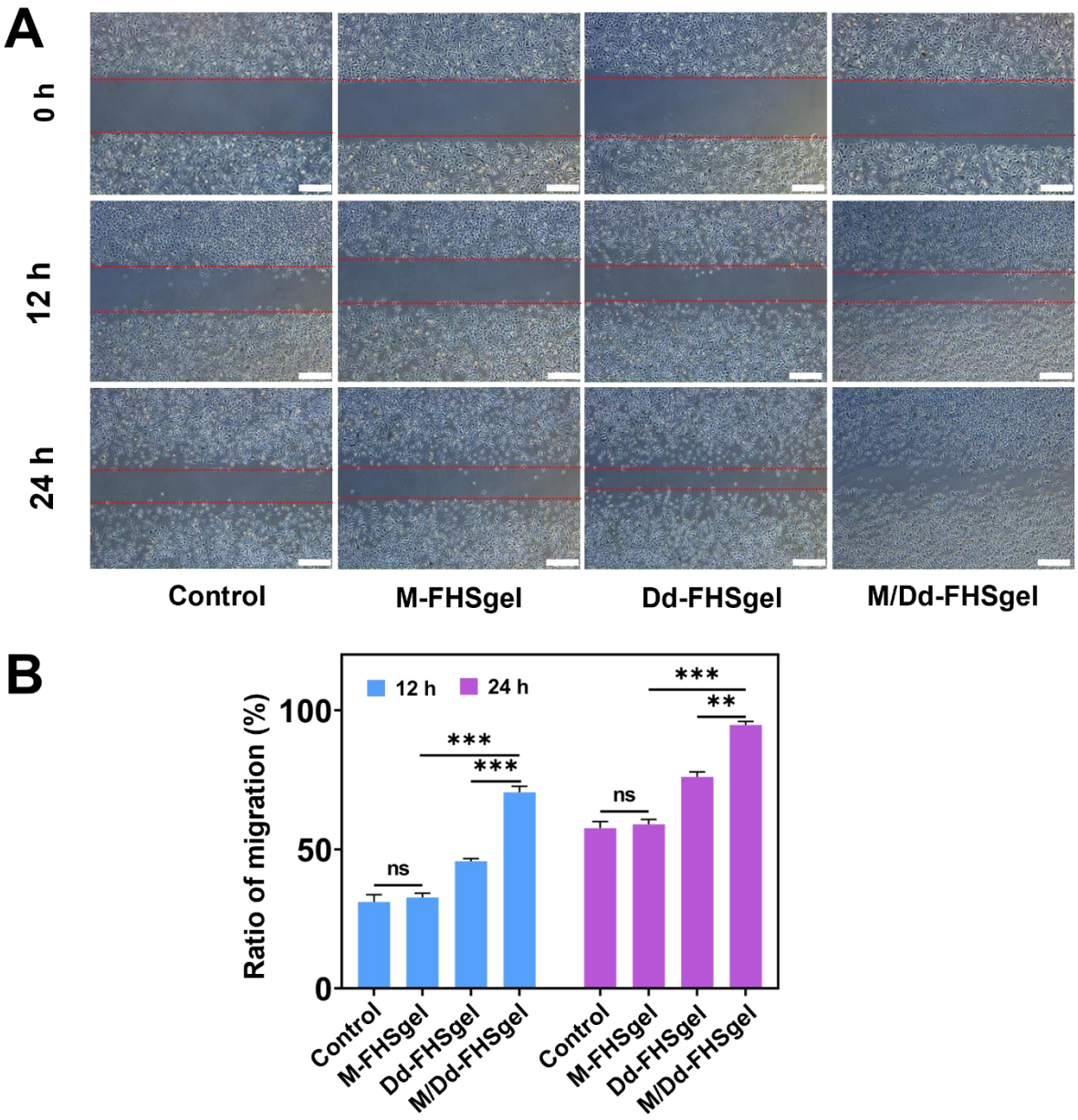

Figure S24. (A) Migrations of L929 in response to various treatments at 0 h, 12 h and 24 h (Scale bar = 200 μm). (B) Quantitative analysis of migration rate. Data are means ± s.d. (n = 3). *$p < 0.05$, **$p < 0.01$, ***$p < 0.001$. *ns* represents no statistical difference.

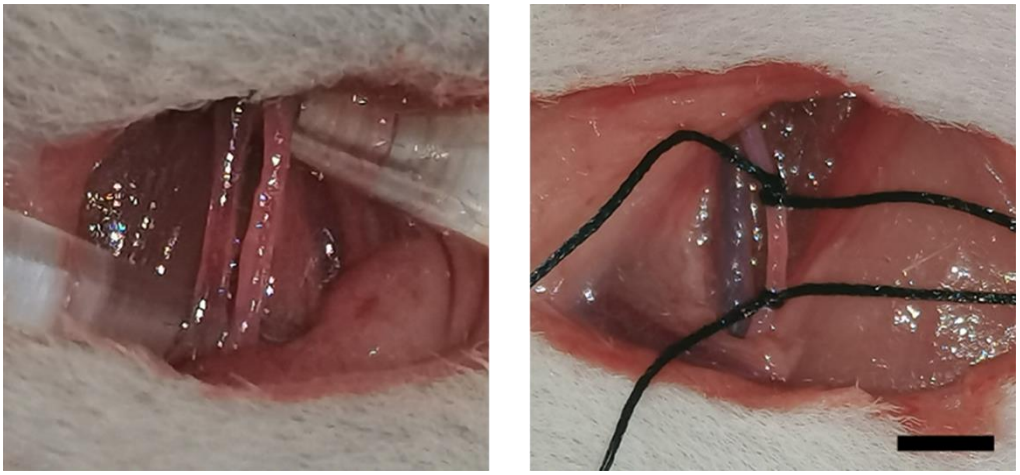

Figure S25. Optical images of limb ischemia model (Scale bar = 1 cm).

Figure S26. Optical images of FHSgel with different temperatures (Scale bar = 1 cm).

Figure S27. Optical image of gastrocnemius muscle (Scale bar = 1 cm).

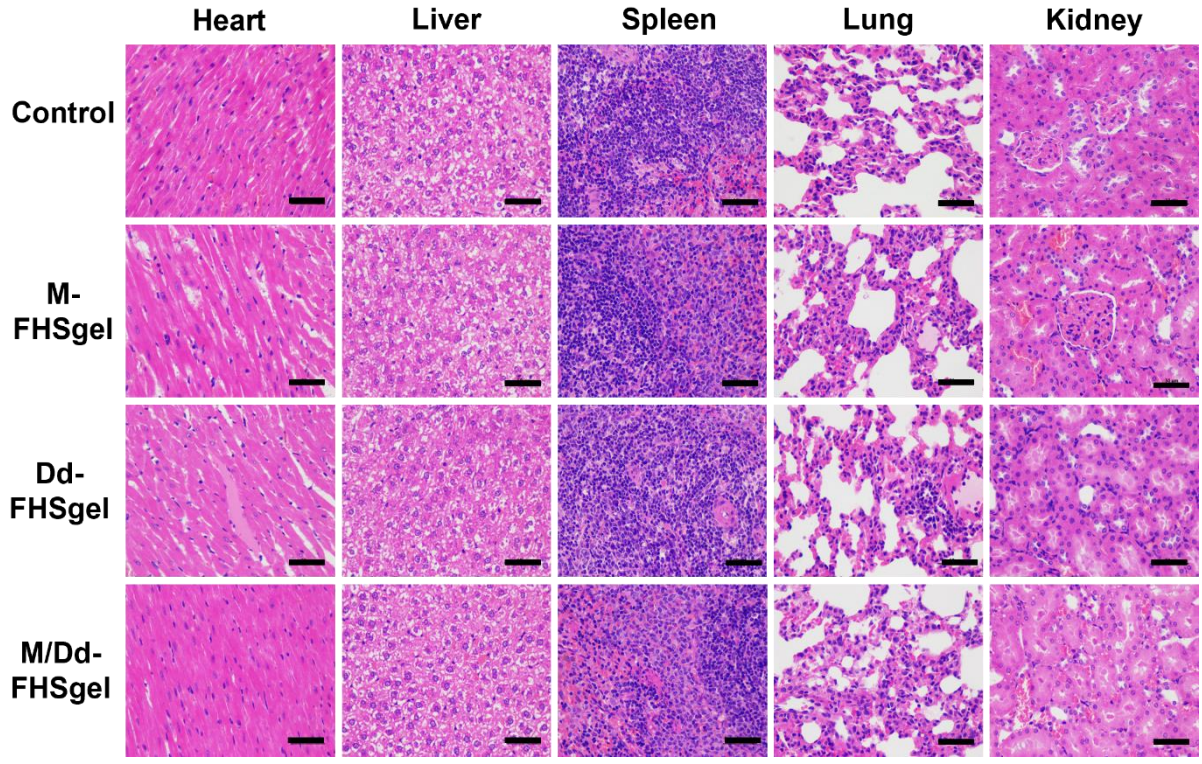

Figure S28. H&E staining of main organs after different treatment (Scale bar = 100 μm).